Reinforcement Learning-Tuned Fractional-Order Sliding Mode Control for Load Frequency Stability in Power Systems

Farhad Amiri1*

Department of Electrical Engineering, Tafresh University, Tafresh 39518-79611, Iran, f.amiri@tafreshu.ac.ir

Abstract: Power systems can improve their frequency stability by using the load-frequency control (LFC) system. Power system parameter unpredictability and unforeseen load disruptions complicate and test the LFC system's performance. The goal of this work is to increase the frequency stability of a two-area power system by constructing the fractional-order sliding mode controller (FOSMC) inside each area's LFC structure. The controller is combined with reinforcement learning (RL) to further enhance the FOSMC's performance against disturbances and parameter uncertainty. The primary objective of this control strategy is to enhance dynamic performance and reduce frequency oscillations in the face of unforeseen load interruptions and uncertainty in all power system components. The performance of the SMC is improved by utilizing fractional derivatives in the sliding surface, which successfully reduces chattering and raises the frequency stability of the two-area power system. The performance of the suggested method is assessed in the context of LFC for power systems under various situations by contrasting it with alternative control strategies, such as PDSMC, SMC and Fuzzy-RL. The findings show that the suggested method (FOSMC-RL) significantly improved the frequency stability of the two-area power system. Additionally, the suggested approach shows resilience to high power system parameter uncertainty and severe abrupt load disruptions.

Keywords: Fractional order sliding mode control, RL, chattering, power system, sudden changes,

1- Introduction

Frequency regulation is one of the most crucial aspects of the power system to guarantee the reliability and caliber of power supplied to customers [1]. Frequency regulation in power networks with two or more areas is a complicated problem [2]. These systems consist of several regions connected by transmission lines, each of which has a load, governor, turbine, synchronous generator, etc. [3, 4]. Abrupt variations in load in each region of a multi-area power system have a direct impact on the frequency of that area and adjacent areas, and they may also have an impact on the power exchange between areas [5-7]. Frequency variation from the nominal value can compromise the power system's frequency stability and cause major equipment damage [8]. The primary issue in a multi-area power system is frequency regulation, as variations in one area's frequency have a rapid impact on other regions, leading to variations in communication line power [9, 10]. An LFC system has been employed to preserve and enhance the multi-zone power system's frequency stability. Several controllers have been employed in the load-frequency system's construction; each one's benefits and drawbacks are covered below [11–27].

In [11, 12], the MPC is used in the LFC structure of the multi-area power system. Although the MPC is robust to the unpredictability of the system's features, it performs poorly against disturbances that enter the multi-area power system. In [13], the LFC system of a multi-area power system is structured using a fuzzy controller, and in [14], a neural-fuzzy controller. The fuzzy controller's performance is adequate for dealing with the multi-area power system's parameter uncertainty, but it struggles when load disruptions occur. Against uncertainty, the neural-fuzzy controller performs better. Although this approach is likewise resilient to disruptions, its great computing complexity makes it troublesome in real time. The LFC structure of the multi-area power system employed the PID controller optimized with the rabbit algorithm in [15], and the

AUT Journal of Electrical Engineering 10.22060/eei.2025.24314.5680

PID controller optimized with the GA and PSO in [16,17]. The PID controller performs effectively when there are load disruptions, but it will produce instability when there is parameter uncertainty. The LFC structure of the multi-area power system employed the FOPID controller in [18, 19], and in [20], the FOPID controller was optimized with the GWO. The FOPID controller is not robust against extreme uncertainty, but it performs well against load disturbances and mild power system parameter uncertainty. The LFC structure of a multi-area power system uses the PI-PD cascade controller in [21], the fractional-order fuzzy PID controller in [22], and the FOPID-1+TD cascade controller in [23]. Although the cascaded controller is resilient to uncertainty, it is not resilient to significant load disruptions. The SMC is utilized in [24–26] to enhance the LFC system's performance inside a multi-area power system framework. The SMC uses the sign function to reach the sliding level and deal with disturbances, which will cause damage to the power system components and chattering (high-frequency oscillations). The performance of the sliding mode control is good against mild parameter uncertainty and mild load disturbances in the power system, but it is not robust against severe uncertainty and severe load disturbances. In a multi-area power system configuration, the PDSMC is utilized in [27] to enhance the LFC system's performance. Additionally, this controller is not resilient to extreme power system parameter variability. In order to increase the dynamic performance and frequency stability of a multi-area power system, a controller that is resilient against severe disturbances and extreme parameter uncertainty must be included into the LFC system.

In this paper, the FOSMC is created in the LFC system of each power system region to enhance the frequency stability of the two-area power system. The following are some justifications for integrating the FOSMC with RL:

- The FOSMC has a good performance against disturbances and uncertainties due to its robust structure. However, precise adjustment of control coefficients under different environmental conditions is a major challenge. RL can automatically and dynamically adjust these coefficients and improve the system performance in the presence of severe changes and uncertainties.
- One of the fundamental problems of SMC is chattering, which causes unwanted oscillations and even damage to the system. Using a FOSMC reduces this problem, but in some special situations, it is necessary to optimize the sliding surface coefficients. RL helps to automatically adjust these coefficients and further improves the reduction of chattering.
- Power systems often operate under variable conditions and their dynamic characteristics change under the influence of loading and disturbances. RL provides the ability to learn and adjust the controller online by using real-time system data.

This control method's primary goal is to enhance dynamic performance and lessen frequency variations in each section of the power system when there are unexpected load disruptions and uncertainty. In this control method, by using fractional derivatives in the sliding surface, the performance of sliding mode control is improved, the chattering problem is reduced and the frequency stability of the two-area power system is improved.

The performance of the proposed method is compared with other control methods (PDSMC, SMC, Fuzzy-RL) in the field of LFC of the power system by considering various scenarios and presenting the results of using the suggested method (FOSMC-RL) to improve the frequency stability of the two-area power system.

Additionally, the suggested approach can tolerate very abrupt load fluctuations and extreme power system parameter uncertainty. The following lists the paper's contributions:

- 1. Design of the FOSMC for a two-area Power System.
- 2. Integration of RL with FOSMC.
- 3. Improvement of Frequency Control Performance in a two-area Power System:

4. Providing Several Comprehensive Comparative Methods to Compare the Performance of the Proposed Method:

The paper consists of several sections: In section (2), the studied power system is described. In section (3), the design of FOSMC based on RL for the two-area power system with disturbances and complementary control error (ACE) is described. In sections (4) and (5), the simulation and conclusion are presented, respectively.

2- The studied power system

The two-area power system model is displayed in Fig. 1. The governor, steam turbine, and generator are all components of the power system under study; in the governor model, the dead band is taken into account, and in the steam turbine model, the production rate limit is taken into account. Table 1 displays the characteristics associated with the two-area power system. The governor-related transfer function is presented in Eq. (1) [24–26].

$$G_H(s) = \frac{1}{T_{Gi}s + 1}, i = 1, 2$$
 (1)

In Eq. (1), T_{Gi} is the governor time constant for area i of the power system. In Eq. (2), the transfer function for the steam turbine is shown [27].

$$G_T(s) = \frac{1}{T_{ii}s + 1}, i = 1, 2$$
 (2)

The steam turbine's time constant for area i of the power system is represented by T_{ti} in Eq. (2). Eq. (3) displays the associated transfer function for the generator.

$$G_P(s) = \frac{k_{Pi}}{T_{Pi}s + 1} \tag{3}$$

Eq. (3) uses the symbols k_{pi} and T_{pi} to represent the gain and time constant of the power system of area i, respectively. The communication error's power deviations are displayed in Eq. (4) [27].

$$\Delta P_{tie_{ij}} = 2\pi T_{ij} \left(\int_{0}^{t} \Delta f_{i} dt - \int_{0}^{t} \Delta f_{j} dt \right)$$
(4)

In Eq. (4), T_{ij} is the coefficient of the connection line between the two-area power systems. In Eq. (5), the complementary control error corresponding to areas (1) and (2) is shown [27].

$$ACE_{i} = \sum_{i=1,2,i\neq n} \Delta P_{tie_{in}} + \beta_{i} \Delta f_{i}$$
(5)

ACE is the complementary control error and β is the frequency bias of the power system in Eq. (5).

Eqs. (1) to (5) for each area of the power system yield the state space relationship of the power system of area (1) and area (2), which is then shown using Eqs. (6) and (7).

$$x = Ax(t) + Bu(t) + Dd(t)$$

$$y = Cx(t)$$
(6)

In Eq. (6), the state vector is denoted by x(t), the system matrix by A, the system input vector by B, the control input by u(t), the disturbance-related vector by D, and the external disturbances that impact the system by d(t). The power of the communication line between two areas is represented by $\Delta P_{tie,i}$ in Eq. (7), the generator output power variation of area i is represented by ΔP_{Gi} , the mechanical power variation by ΔP_{mi} , the frequency deviation by Δf_i , the load variation by ΔP_{Li} , the control signal of area i by ΔP_{Ci} , and the exchange control signal between areas (1) and (2) of the power system by Δv_i .

$$\begin{bmatrix} \Delta \dot{P}_{gi} \\ \dot{\Delta} \dot{P}_{mi} \\ \Delta \dot{f}_{i} \\ \Delta \dot{P}_{tie,i} \end{bmatrix} = \begin{bmatrix} \frac{-1}{T_{gi}} & 0 & \frac{-1}{R_{i}T_{gi}} & 0 \\ \frac{1}{T_{ti}} & -\frac{1}{T_{ti}} & 0 & 0 \\ 0 & \frac{k_{Pi}}{T_{Pi}} & \frac{-1}{T_{Pi}} & -\frac{k_{Pi}}{T_{Pi}} \\ 0 & 0 & 2\pi \sum_{\substack{j=1 \\ j \neq i}} T_{ij} \Delta f & 0 \end{bmatrix} \begin{bmatrix} \Delta P_{gi} \\ \Delta P_{mi} \\ \Delta f_{i} \\ \Delta P_{tie,i} \end{bmatrix} + \begin{bmatrix} \frac{1}{T_{gi}} \\ 0 \\ 0 \\ 0 \end{bmatrix} [\Delta P_{ci}] + \begin{bmatrix} 0 & 0 \\ 0 & 0 \\ -\frac{k_{Pi}}{T_{Pi}} & 0 \\ 0 & -2\pi \end{bmatrix} \begin{bmatrix} \Delta P_{Li} \\ \Delta v_{i} \end{bmatrix}$$

$$y = ACE = \begin{bmatrix} 0 & 0 & \beta_i & 1 \end{bmatrix} \begin{bmatrix} \Delta P_{gi} \\ \Delta P_{mi} \\ \Delta f_i \\ \Delta P_{tie,i} \end{bmatrix}$$

(7)

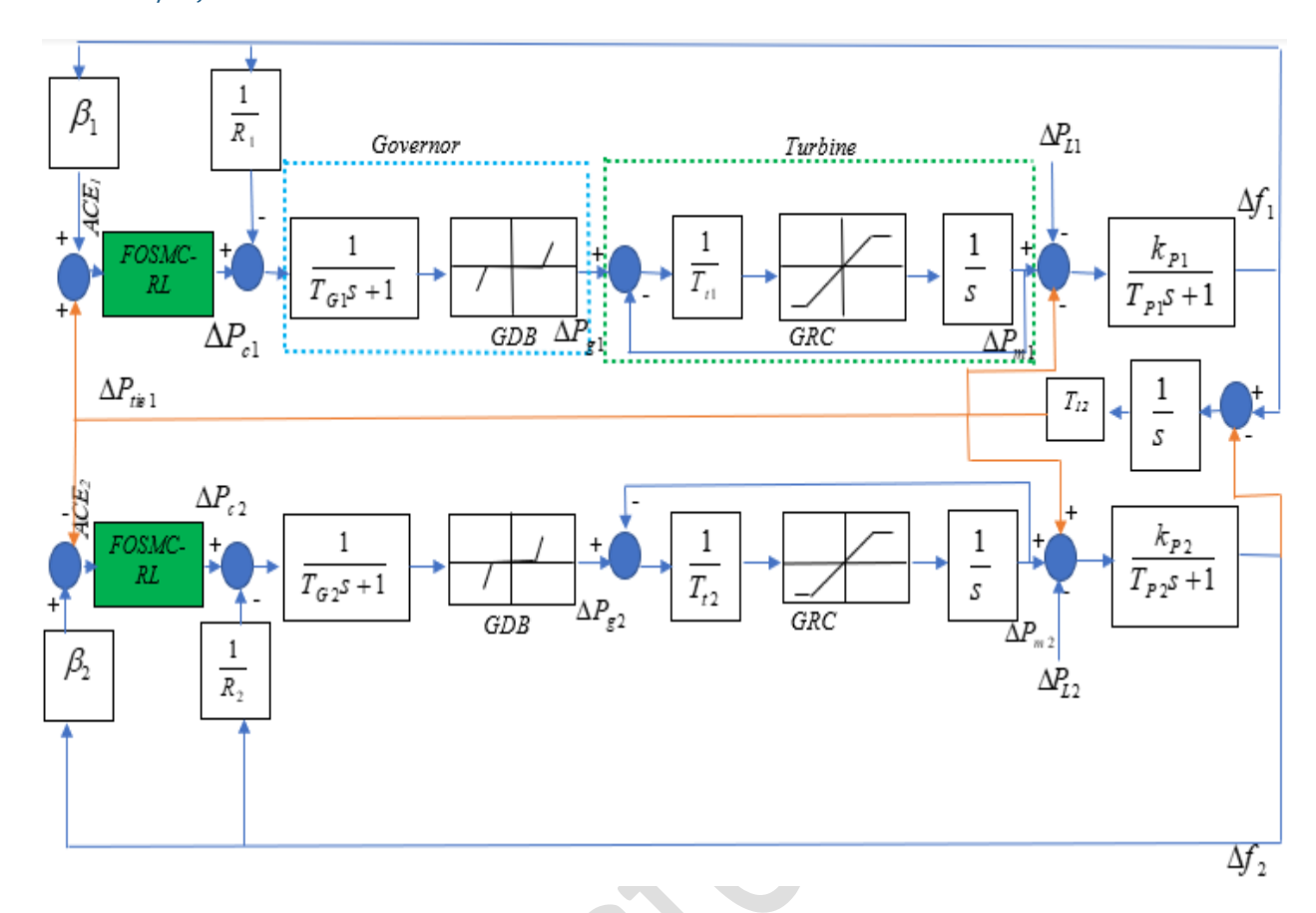


Fig. 1. the model of the two-area power system is shown.

Table 1. Parameters related to the two-area power system [24-26].

Parameter	Area (1)	Area (2)
k_{pi}	120 Hz/pu. MW	115 Hz/pu. MW
T_{pi}	20s	20s
T_{Gi}	0.08s	0.06s
T_{ti}	0.40s	0.44s
β	0.3483pu/Hz	0.3827pu/HZ
Tij	0.20 pu/Hz	0.20 pu/Hz
R	3Hz/pu	2.73Hz/pu

3. The design of FOSMC based on RL for the two-area power system with disturbances and ACE

3-1-FOSMC

FOSMC is a combination of SMC theory and fractional calculus. In the design of this method, fractional derivatives and integrals are used in the definition of the sliding surface. This controller has many advantages due to its greater flexibility in adjustments and response to nonlinear and uncertain conditions of systems. The use of fractional derivatives in SMC improves stability and reduces sensitivity to external disturbances. FOSMC has less chattering (unwanted oscillations) than classical SMC and hence provides better performance in sensitive and nonlinear systems. The fractional parameters of the controller provide more adjustability, which can be useful for complex and uncertain systems.

10.22060/eei.2025.24314.5680

This controller is appropriate for enhancing the performance of systems with intricate and varied dynamic behavior and may be utilized in mechanical, robotic, electrical, etc. systems. The power systems in areas (1) and (2) are examined initially in this study; disruptions have an impact on both areas. In addition, the ACE error is included as a control input in the system, and an FOSMC is designed to control this system.

This power system's strong controller design is the goal. Eqs. (6) and (7) are used to define the state-space equations of the power system of areas (1) and (2).

The aim of the design of a FOSMC is to provide robust control for each area of the system based on the ACE error of the power system and to compensate for disturbances. The error of each area of the power system is defined according to Eq. (5). For this system, it is assumed that the error e(t) is related to the ACE according to Eq. (8).

$$e(t) = ACE \tag{8}$$

The fractional slip surface s(t) is defined using the state error e(t). This fractional slip surface is considered as Eq. (9) [28-30].

$$s(t) = D^{\alpha}e(t) + ce(t)$$

In Eq. (9), e(t)=x(t)-xd(t) is the error between the present and intended states, c is a positive coefficient, D^{α} is the fractional derivative of order α , and Eq. (10) defines the fractional derivative.

$$D^{\alpha}f(t) = \frac{1}{\Gamma(1-\alpha)} \frac{d}{dt} \int_{0}^{t} (t-\tau)^{-\alpha} f(\tau) d\tau$$
(10)

In Eq. (10), $\alpha \epsilon(0,1)$ and $\Gamma(0)$ are gamma functions. FOSMC consists of two parts: the equivalent part (u_{eq}) and the switching part (u_{sw}). To control the system and stay on the sliding surface, first the equivalent part of the control is designed as Eq. (11). The equivalent part is designed because it must compensate for the system dynamics and reduce the system error:

$$u_{eq} = -(B^T B)^{-1} B^T (Ax(t) + Dd(t))$$
(11)

Eq. (11) is equivalent to the force that keeps the system on the slip surface. The switching section is designed to guide the system towards the slip surface and is defined using the slip surface symbol s(t) according to Eq. (12).

$$u_{sw} = -K . sign(s(t))$$
(12)

In Eq. (12), K is the switching coefficient and its value should be chosen such that the system quickly reaches the sliding surface and sign(s(t)) is the sign function that determines the direction of the system's motion. Finally, the general control law is defined as a combination of two equivalent and switching parts according to Eq. (13). To prove the stability of the system using fractional-order sliding control, the Lyapunov function is used. The Lyapunov function is defined as Eq. (14).

$$u(t) = u_{eq} + u_{sw} \tag{13}$$

$$V(s) = \frac{1}{2}s^{2} \tag{14}$$

The time derivative of Eq. (14) is defined as equation (15).

$$\overset{\bullet}{V}(s) = s \overset{\bullet}{s} \tag{15}$$

Given that s(t) is defined according to Eq. (9), the derivative of this equation is shown in Eq. (16).

$$\dot{s} = D^{\alpha+1}e(t) + c\dot{e}(t) \tag{16}$$

According to the switching control law according to Eq. (12), the derivative of the slip surface is defined as Eq. (17). Consequently, Eq. (18) displays the derivative of the Lyapunov function.

$$\dot{s} = -K . sign(s) \tag{17}$$

$$\dot{V}(s) = s.(-K.sign(s)) = -K|s| \tag{18}$$

Since V(s) is always negative, the Lyapunov function decreases and the system is stable. This indicates that the error e(t) will converge to zero over time and the system will remain on the slip surface.

3-2- Reinforcement Learning:

RL is a method of learning that is predicated on how an agent interacts with its surroundings. Through information from the environment, the agent determines the optimal path of action. The main goal of reinforcement learning is to maximize the cumulative reward over time. The environment reacts by returning the new state and reward once the agent selects an action at each step based on the decision-making policy and the current state. The following are the primary elements of RL [31, 32]:

- ✓ An agent is a creature that is capable of learning.
- ✓ Environment: The outside environment that an agent interacts with.
- \checkmark State (s): The agent is shown the most recent environmental information.
- ✓ Action (a): The agent's choice or behavior in a certain situation.
- \checkmark Reward (r): The agent's input from the surroundings.
- ✓ Policy $(\pi(a|s))$: The direction the agent follows while making decisions.
- \checkmark The action-value function Q(s,a): The anticipation of an action-state's future cumulative reward.

The mean of the eventual incremental reward that the agent anticipates beginning from state s is the value function of a particular state (V(s)), which is illustrated in equation (19).

$$V(s) = E\left[\sum_{t=0}^{\infty} \eta^{t} r_{t} \left| s_{0} = s \right.\right]$$
(19)

In Eq. (19), r_t represents the reward at time t, whereas η , the discount factor, reduces the impact of later rewards ($0 \le \eta \le 1$).

10.22060/eei.2025.24314.5680

The value of a state-activity pair and the amount of cumulative reward that would be anticipated if the agent in state s performed action a and then complied with policy π are provided by the state-action value function (Q(s,a)), which is represented by Eq. (20) [31–33].

$$Q(s,a) = E\left[\sum_{t=0}^{\infty} \eta^{t} r_{t} | s_{0} = s, a_{0} = a\right]$$
 (20)

One of the most famous RL algorithms is Q-Learning, which iteratively updates the value function (Q(s,a)) according to Eq. (21) [34].

$$Q(s,a) \leftarrow Q(s,a) + \tau \left[r + \eta \max Q(s',a') - Q(s,a) \right]$$
(21)

In Eq. (21), a' is the best course of action in the next state, s' is the next state, and τ is the learning rate.

The reward function in reinforcement learning should reflect the target performance of the system. To control the power system, a reward function of the following form is used according to Eq. (22) ($\lambda = 0.5$).

$$r = -(e(t)^{2} + \lambda u(t)^{2})$$
(22)

Where in Eq. (22), e(t) is the system error over time, u(t) is the control input, and λ is a coefficient for weighting the energy consumption.

According to Eq. (23), the optimal strategy in reinforcement learning (π^*) is the one that gives the agent the most cumulative reward.

$$\pi^*(s) = \arg\max Q(s, a) \tag{23}$$

3-3-FOSMC based on RL

RL is used to adjust the coefficients of the FOSMC. In RL, the state (s) includes the system states e(t) s(t) and s(t). The action (a) of changing the coefficients Δc , $\Delta \alpha$, ΔK is considered. The reward is also calculated according to Eq. (22). Also, using the RL algorithm, the parameters are updated according to Eq. (24).

$$\eta \Delta K + K \leftarrow K
\eta \Delta \alpha + \alpha \leftarrow \alpha
\eta \Delta c + c \leftarrow c$$
... (24)

The improved slip surface is obtained by RL according to Eq. (25).

$$s(t) = D^{\alpha}e(t) + ce(t) + \phi_{RL}(t)$$
(25)

The final control signal is applied based on Eq. (26) by considering the RL effect.

$$u(t) = u_{eq} + u_{sw} + u_{RL}$$
 (26)

The control signal generated by reinforcement learning (u_{RL}) is calculated according to Eq. (27).

$$u_{RL} = \Delta K sign(s(t)) + \Delta ce(t)$$
 ... (27)

Eq. (28) displays the Lyapunov function of the suggested controller (FOSMC based on RL) in order to guarantee stability.

$$V(s,\theta) = \frac{1}{2}s^2 + \frac{1}{2}\theta^T\theta$$
 (28)

In Eq. (28), θ is the vector of RL coefficients (c, α ,K). Eq. (29) is used to compute the Lyapunov function's time derivative.

$$\overset{\bullet}{V}(s,\theta) = s \overset{\bullet}{s} + \theta^T \theta \tag{29}$$

In Eq. (29), by inserting control rules into it, the Lyapunov stability relation for the textual FOSMC based on RL is shown according to Eq. (30). The proposed controller pseudocode to improve frequency stability for power system is given in the Appendix. A. The parameter values of the proposed method are shown in Table 2. The block diagram of the proposed method for controlling the two-area power system is shown in Appendix. B.

$$\dot{V}(s,\theta) = -K |s| - \lambda |\theta|^2 \tag{30}$$

Table 2. The parameter values of the proposed method

Aspect	Specification
Learning Rate (τ)	au = 0.2
α	0.9
С	1
Discount Factor (η)	$\eta = 0.95$
Exploration Strategy	ε -greedy: Initial $\varepsilon = 0.3$, decayed by 0.99 per
	episode. Actions: Random exploration (prob. ε)
	vs. greedy Q-max (prob. $1-\varepsilon$).
RL Structure	Q-table. States discretized into bins: $e(t)$, $\dot{s}(t)$, $s(t)$
	(3 dimensions). Actions: Discrete adjustments
	$[\Delta c, \Delta \alpha, \Delta K]$ with step sizes $[0.1, 0.01, 0.5]$.
initialize_RL()	• Initialize Q-table with zeros (dimensions:
	state bins \times actions)
	• Set hyperparameters: τ =0.2, η =0.95, ε =0.3
	 Initialize state discretization thresholds.
update_policy()	• Discretize current state $s = [e(t), \dot{s}(t), s(t)]$
	 Select action a via ε-greedy: argmax_a
	Q(s,a) or random
	Update Q-table using Equation 21:
Reward Calculation	$r(t) = -[e(t)^2 + 0.5 \cdot u(t)^2]$ (Equation 22, $\lambda = 0.5$)
Action Execution	Apply Δc , $\Delta \alpha$, ΔK to adjust FOSMC parameters
	(Equations 24-25) → Update control signal u
	(Equation 26).

4-Simulation:

To compare the proposed method with current methodologies that have been studied in the field of frequency management of two-area power systems, three scenarios have been considered. The suggested technique (FOSMC-RL) has been evaluated against severe disturbances that enter the two-area power system in scenario (1) versus alternative control techniques (PDSMC, SMC, Fuzzy-RL). The suggested approach has been contrasted with other control strategies in scenario (2) to guard against minor disruptions that might infiltrate the two-area power system. The simultaneous impact of severe disruptions and extreme power system parameter uncertainty has been examined in scenario (3). In scenario (4) is performed to analyze the sensitivity of the effect of changes in the parameters of the proposed controller (α, c, τ) on the power system

4-1-Scenario (1):

In this case, the two-area power system is subjected to the load variations of area (1) based on Fig. 2 and the load variations of area (2) based on Fig. 3. The FR of the two-area power system's area (1) is displayed in terms of the proposed controller (FOSMC-RL), PDSMC, SMC and Fuzzy-RL in Fig. 4, and the FR of the two-area power system's area (2) is displayed in terms of the proposed controller (FOSMC-RL), PDSMC, SMC and Fuzzy-RL in Fig. 5. Figs 4 and 5 demonstrate that the proposed controller has outperformed alternative control strategies and is resilient to severe load disturbances pertaining to area (1) and area (2) of the power system. Additionally, the suggested approach has a shorter settling time and has been successful in lowering the frequency deviations associated with areas (1) and (2) of the power system. The outcomes pertaining to scenario (1) are displayed in Table 3.

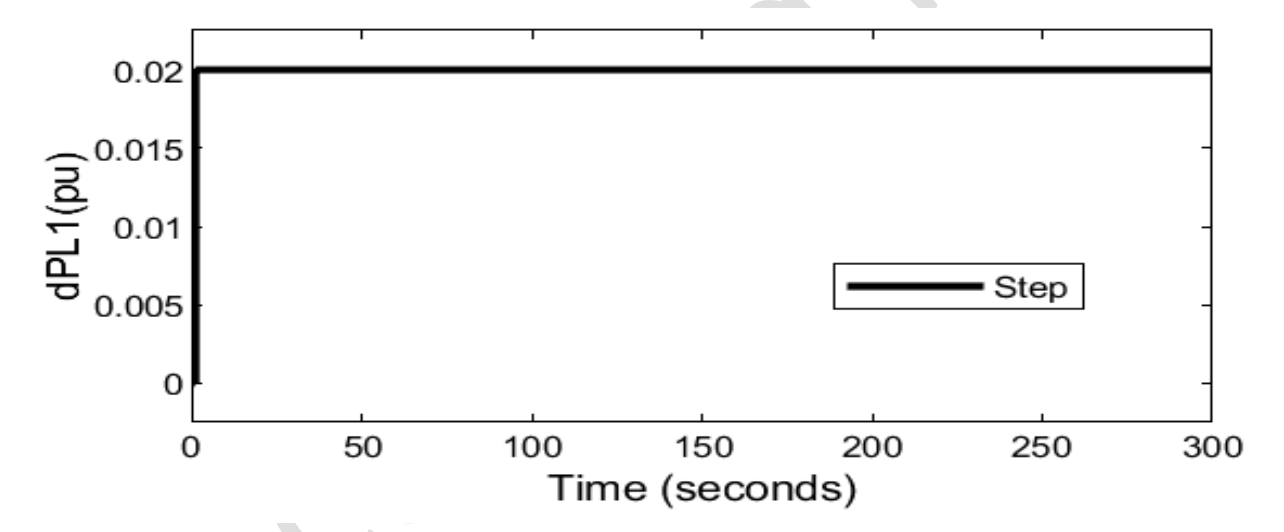


Fig. 2. Load variations of area (1) of the power system, scenario (1)

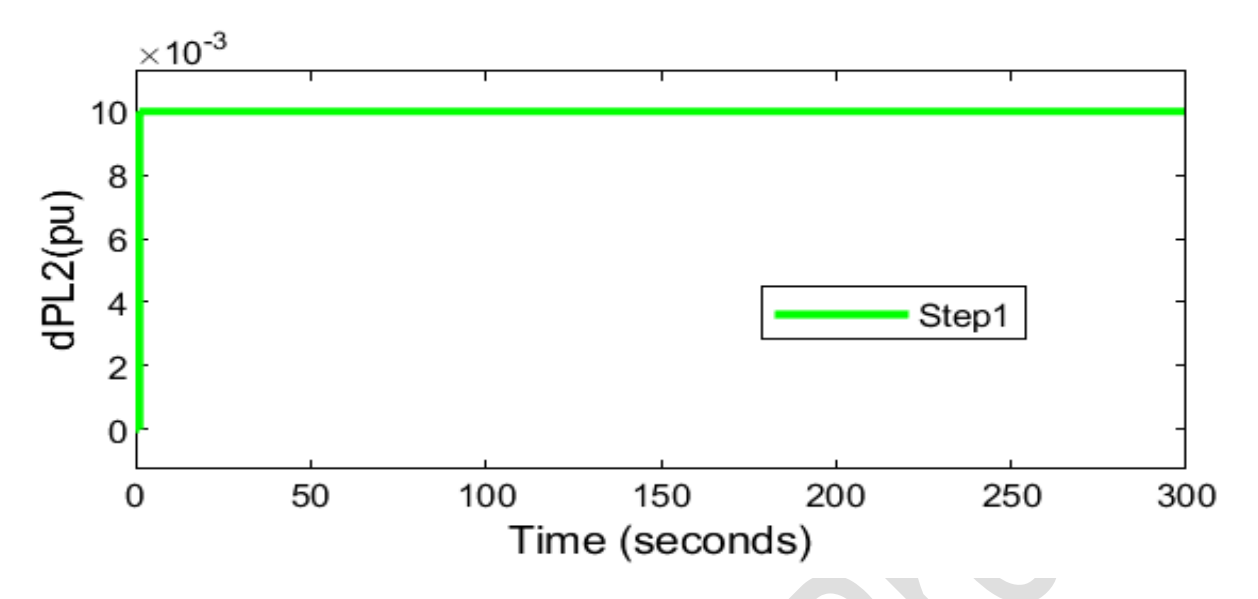


Fig. 3. Load variations of area (2) of the power system, scenario (1)

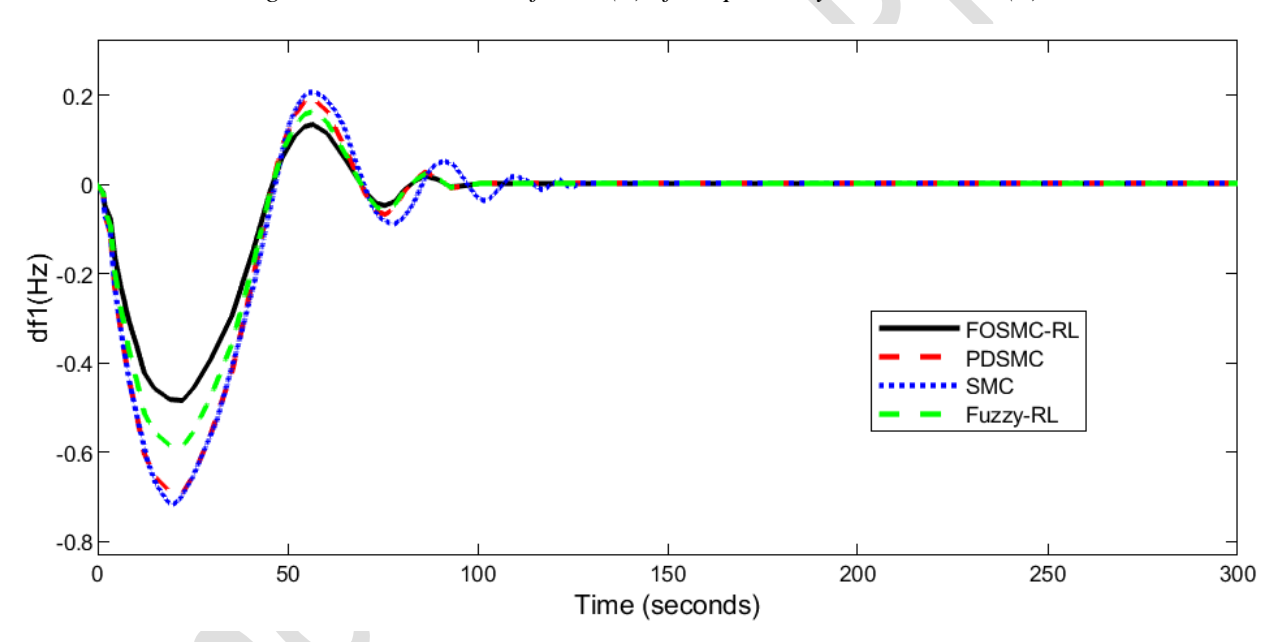


Fig. 4. The FR of area (1) of the two-area power system, scenario (1)

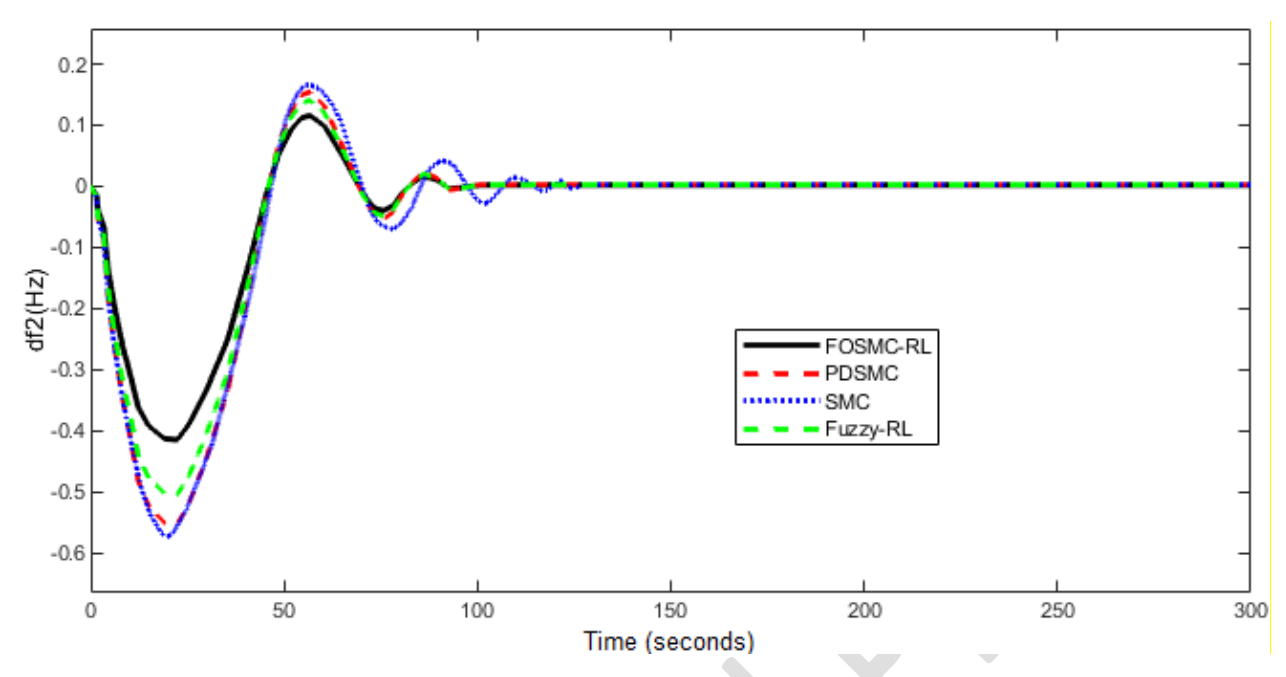


Fig. 5. The FR of area (2) of the two-area power system, scenario (1)

Table 3. Results of Scenario (1)

Controller	Δf_1			Δf_2		
	MO (Hz)	MU (Hz)	ST (sec)	MO (Hz)	MU (Hz)	ST (sec)
FOSMC- RL	0.15	0.45	76	0.10	0.40	75
PDSMC	0.19	0.70	84	0.16	0.56	82
SMC	0.20	0.70	120	0.14	0.54	120
Fuzzy-RL	0.17	0.60	83	0.13	0.50	82

4-2-Scenario (2):

In this instance, the load fluctuations of area (1) as shown in Fig. 6 and the load variations of area (2) as shown in Fig. 7 are applied to the power system. The two-area power system's FR of area (1) is displayed in Fig. 8 in terms of the suggested controller (FOSMC-RL), PDSMC, SMC and Fuzzy-RL. The FR of the two-area power system's area (2) is displayed in Fig. 9 in terms of the suggested controller (FOSMC-RL PDSMC, SMC and Fuzzy-RL. The suggested controller has outperformed alternative control strategies and is resilient to minor load disruptions associated with areas (1) and (2) of the power system, as shown in Figs 8 and 9.

Additionally, the suggested approach has a shorter settling time and has been successful in lowering the frequency deviations associated with regions (1) and (2) of the power system. In Table 4, the results related to scenario (2) are shown.

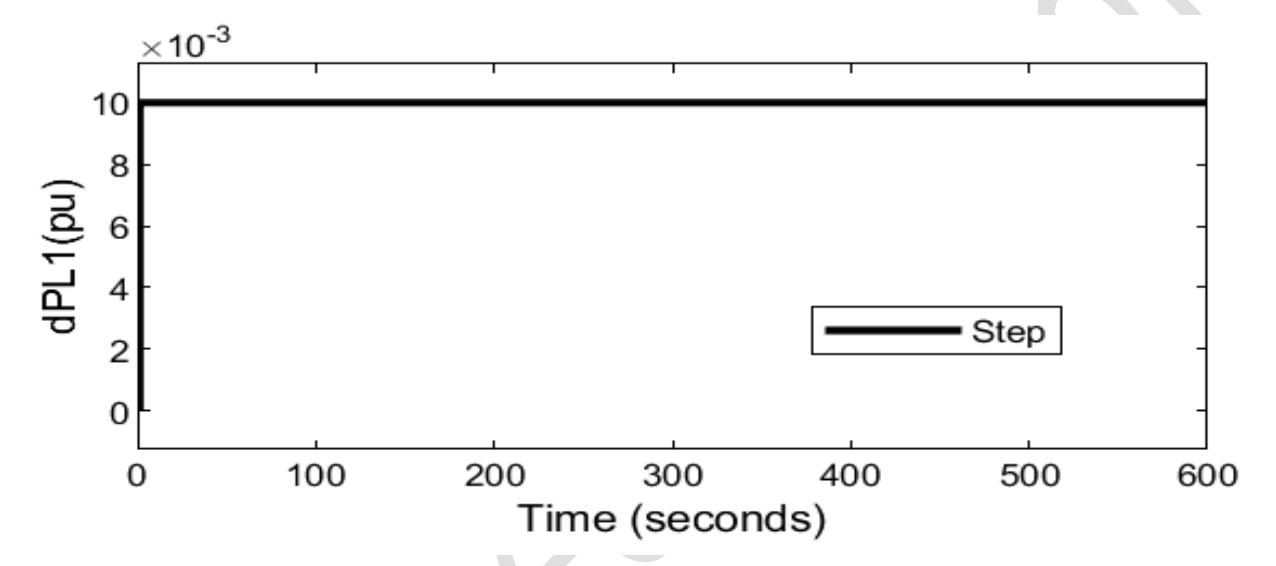


Fig. 6. Load variations of area (1) of the power system, scenario (2)

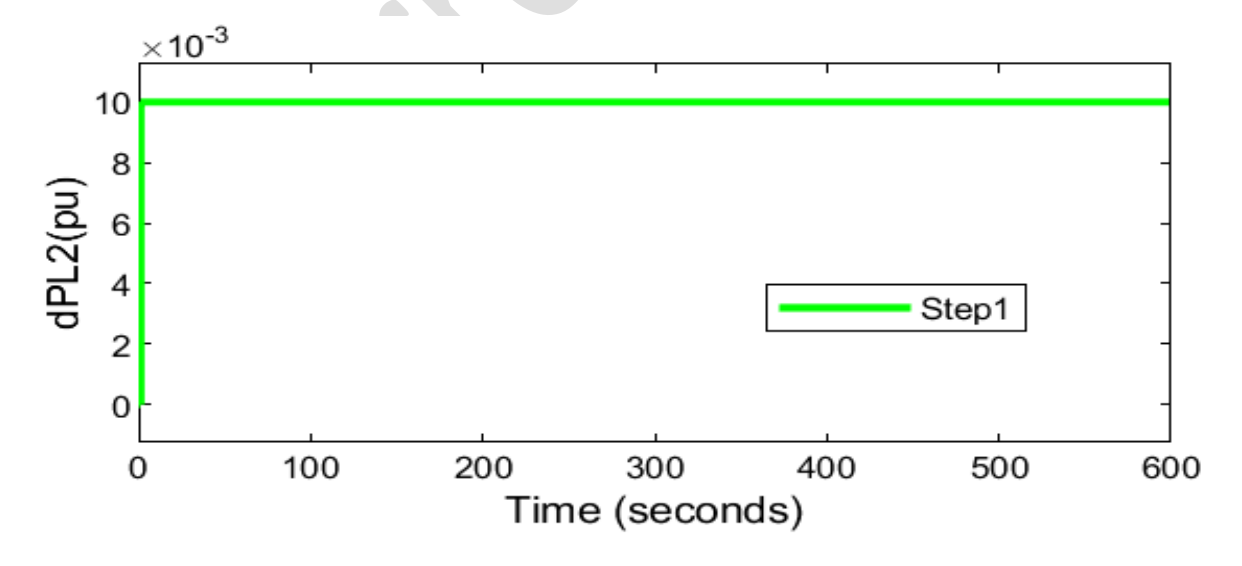


Fig. 7. Load variations of area (2) of the power system, scenario (2)

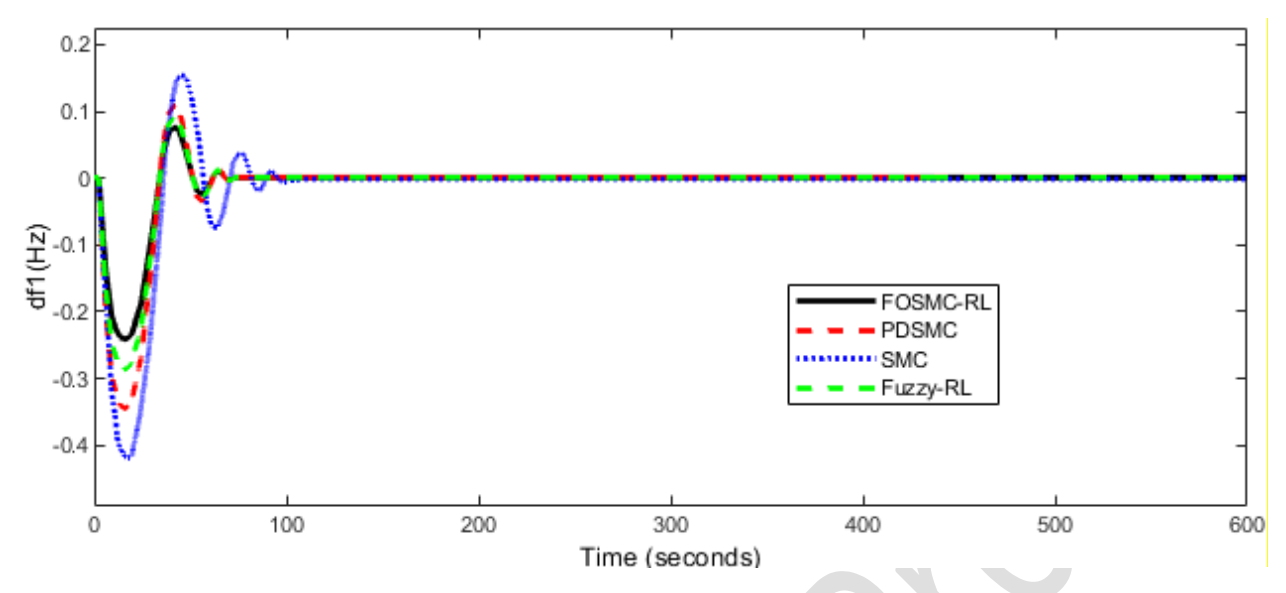


Fig. 8. The FR of area (1) of the power system, scenario (2)

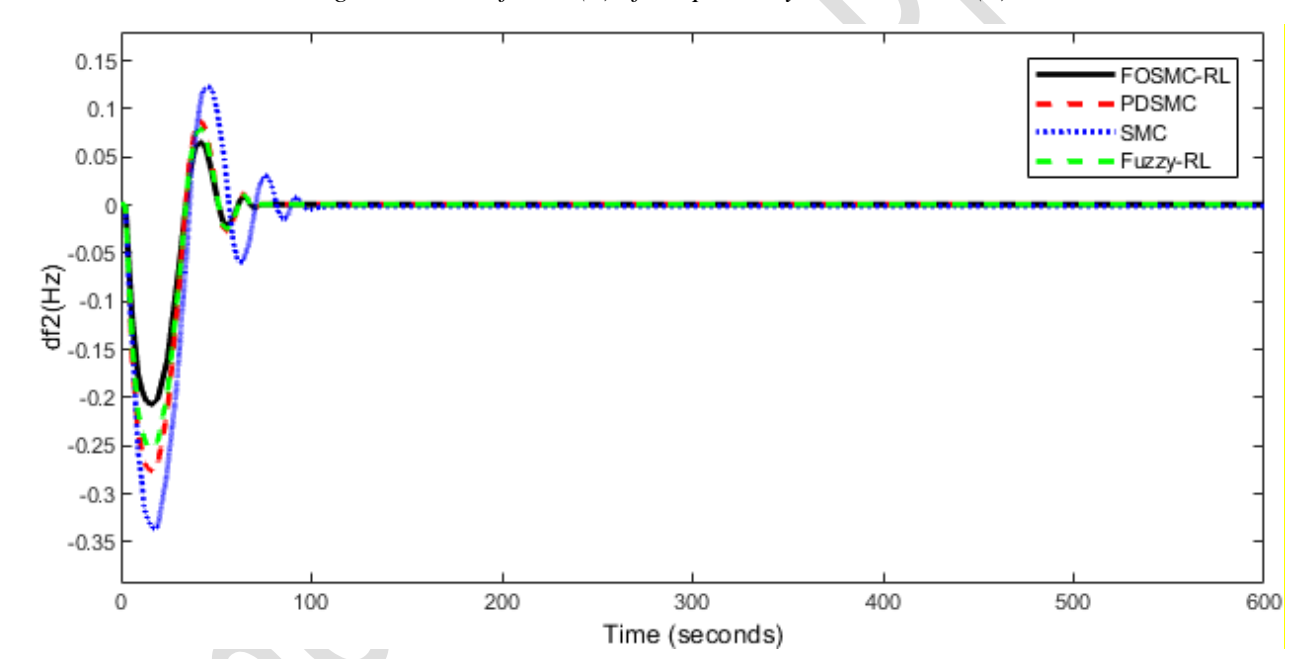


Fig. 9. The FR of area (2) of the power system, scenario (2)

Table 4. Results of Scenario (2)

		$\Delta \mathrm{f}_1$		$\Delta \mathrm{f}_2$		
	MO (Hz)	MU (Hz)	ST (sec)	MO (Hz)	MU (Hz)	ST (sec)
FOSMC-RL	0.08	0.22	67	0.06	0.20	68
PDSMC	0.10	0.35	81	0.08	0.28	80
SMC	0.11	0.43	112	0.15	0.35	113
Fuzzy-RL	0.09	0.28	80	0.078	0.25	80

4-3-Scenario (3):

In this case, the power system is subjected to the load fluctuations of area (1) based on Fig. 2 and the load variations of area (2) based on Fig. 3. Additionally, the impact of extreme uncertainty in the two-area power system's characteristics ($T_{GI}=T_{G2}=+20\%$) is taken into account in this scenario. The FR of area (1) of the power system is displayed in Fig. 10, with respect to the suggested controller (FOSMC-RL), PDSMC, SMC and Fuzzy-RL. The FR of area (2) of the power system is displayed in Figure (11), with respect to the suggested controller (FOSMC-RL), PDSMC, SMC and Fuzzy-RL.

According to Figs. 10 and 11, the suggested controller has outperformed other control strategies and is resilient to significant load disruptions associated with the power system's areas (1) and (2) as well as significant uncertainty in the parameters pertaining to the power system. This technique (FOSMC-RL) has a shorter settling time and has been successful in lowering the frequency deviations associated with areas (1) and (2) of the power system. In Table 5, the results related to scenario (3) are shown.

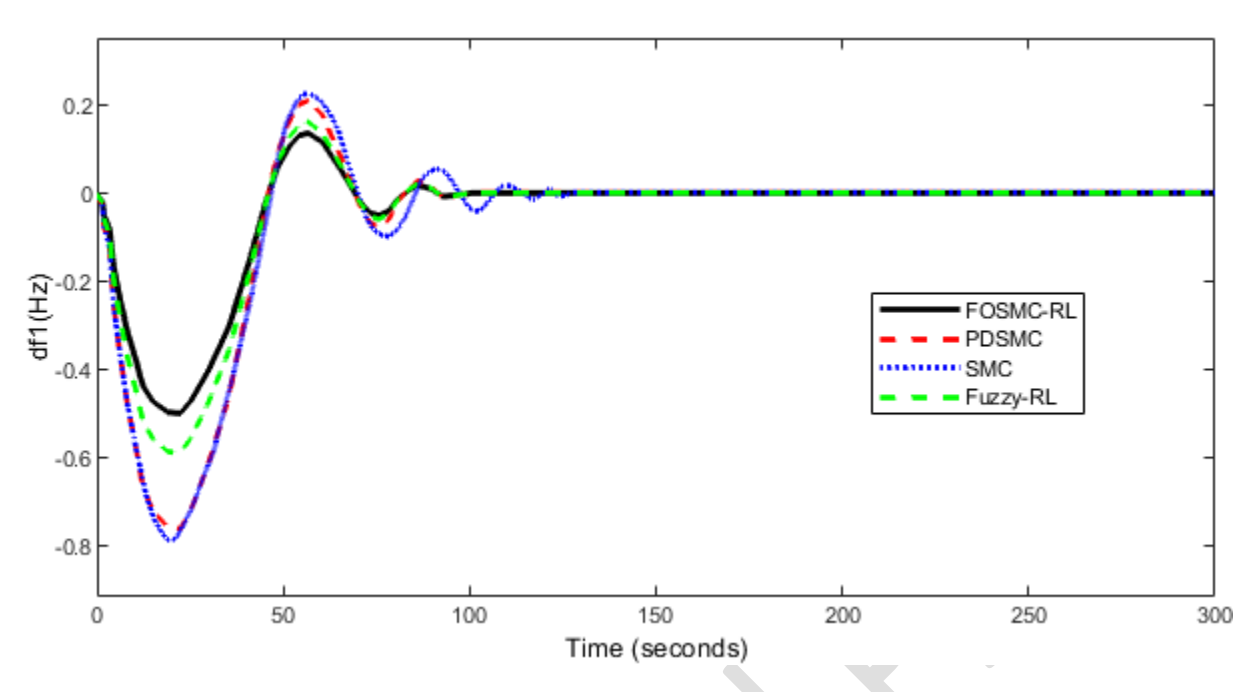


Fig. 10. The FR of area (1) of the power system, scenario (3)

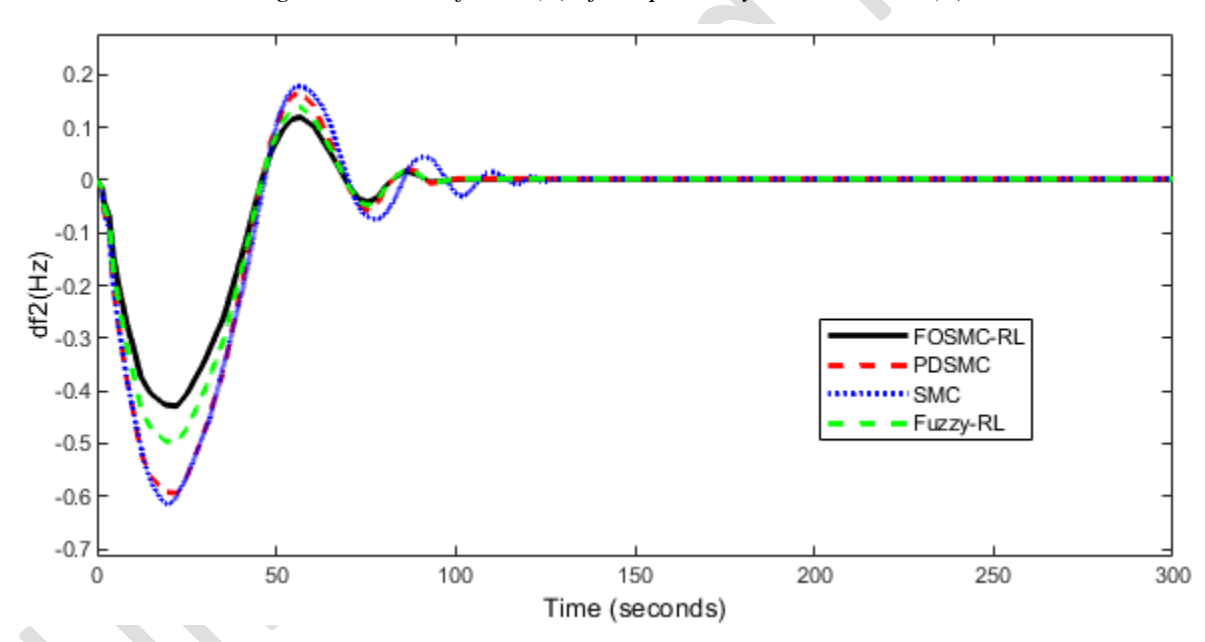


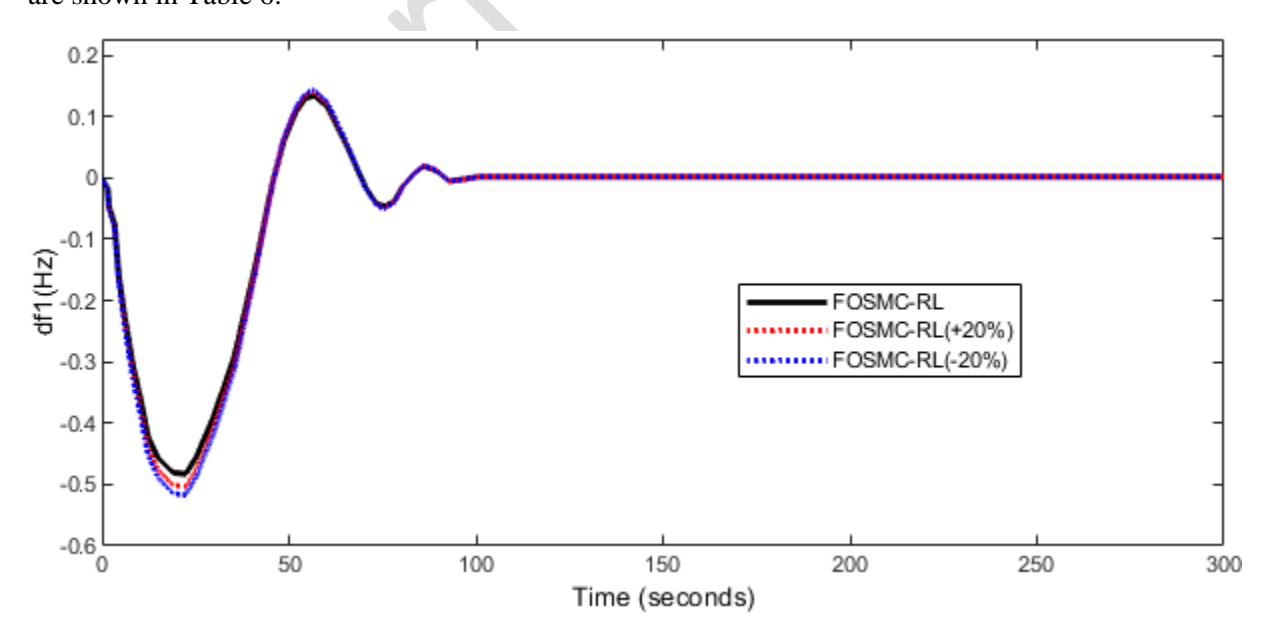
Fig. 11. The FR of area (2) of the power system, scenario (3)

Table 5. Results of Scenario (3)

	$\Delta \mathrm{f}_1$			$\Delta \mathrm{f}_2$		
Controller	MO (Hz)	MU (Hz)	ST (sec)	MO (Hz)	MU (Hz)	ST (sec)
FOSMC- RL	0.16	0.47	77	0.13	0.42	76
PDSMC	0.21	0.77	88	0.20	0.59	89
SMC	0.22	0.78	133	0.21	0.61	135
Fuzzy-RL	0.17	0.60	84	0.13	0.51	83

4-4-Scenario (4):

This scenario is performed to analyze the sensitivity of the effect of changes in the parameters of the proposed controller (α, c, τ) on the power system. The changes in the loads on the two-area power system are as shown in Figs. 2 and 3. The FR of areas (1) and (2) in the power system, considering changes in the parameters of the proposed controller of $\pm 20\%$, are shown in Figs. 12 and 13. The results of this scenario are shown in Table 6.



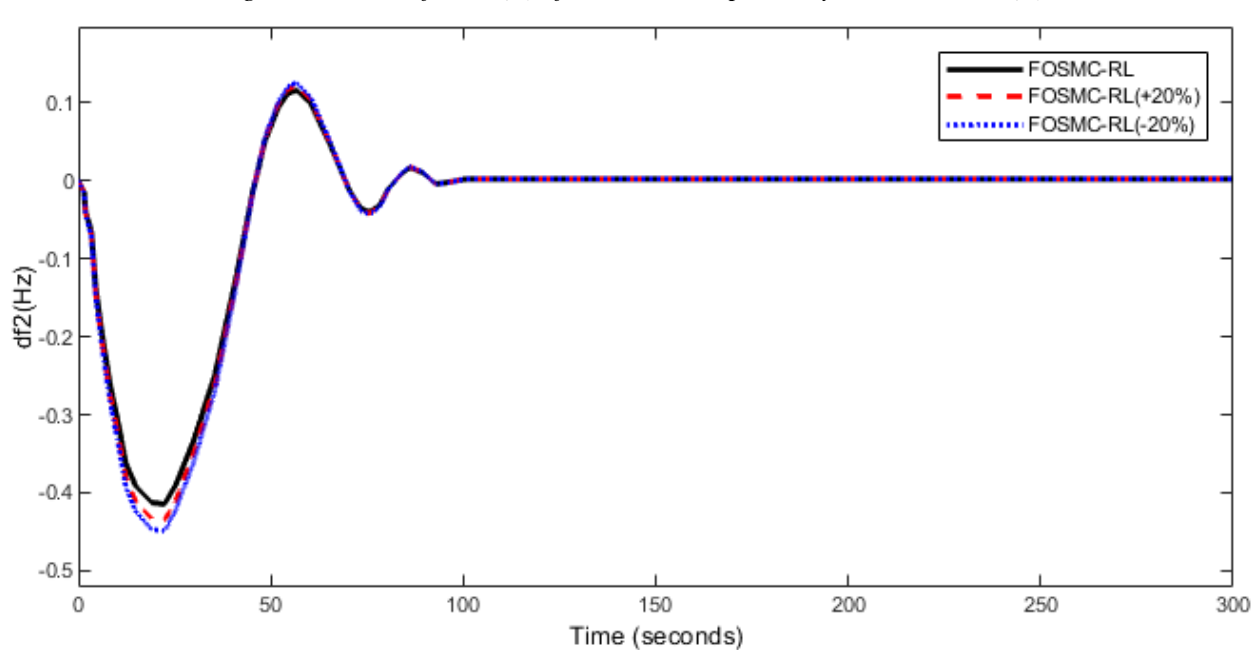


Fig. 12. The FR of area (1) of the two-area power system, scenario (4)

Fig. 13. The FR of area (2) of the two-area power system, scenario (4)

Table 6. Results of Scenario (4)

Controller		$\Delta \mathrm{f}_1$),	$\Delta \mathrm{f}_2$	
	MO (Hz)	MU (Hz)	ST (sec)	MO (Hz)	MU (Hz)	ST (sec)
FOSMC- RL	0.15	0.45	76	0.10	0.40	75
FOSMC- RL(+20%)	0.151	0.49	77	0.11	0.42	75
FOSMC- RL(-20%)	0.153	0.51	77	0.116	0.44	75

According to the results obtained in Table 6, the proposed controller is robust to changes in its parameters and the FR values for areas 1 and 2 of the power system do not change much. Also, the ST for the FR of areas 1 and 2 of the power system remains constant with respect to the changes.

5- Conclusion:

The main goal of this control technique is to improve dynamic performance and reduce frequency variations in the face of unforeseen load disruptions and uncertainty in every part of the power system. In this paper, a FOSMC based on RL was built in the LFC structure of each power system area to improve the frequency stability of the power system. By using fractional derivatives in the sliding surface, this control technique has improved the frequency stability of the two-area power system, reduced chattering, and increased sliding mode control performance. The FOSMC-RL has improved the power system's area 1 and area 2 maximum frequency deviations by 38%. Furthermore, the FOSMC-RL has been used to enhance by 13% the settling time related to frequency changes caused by load disturbances and parameter uncertainties.

Abbreviations:

PDSMC	proportional-derivative
	sliding mode control
MPC	Model Predictive Control
SMC	sliding mode control
GA	Genetic algorithm
PSO	Particle Swarm Algorithm
GWO	Grey Wolf Optimization
FR	Frequency response
MO	Maximum overshoot
MU	Maximum undershoot

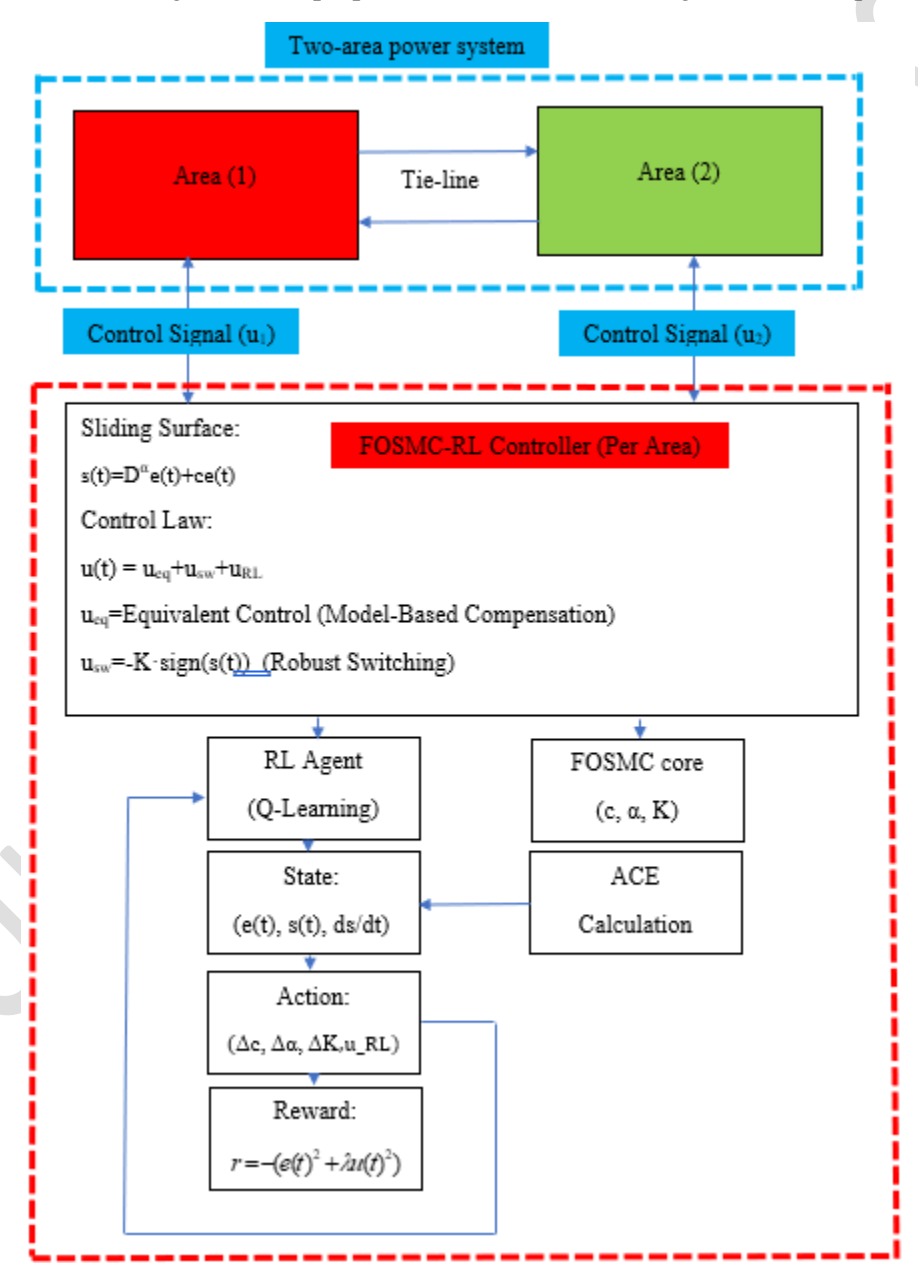
Appendix. A. The pseudocode for the suggested approach.

```
% Initialization
clear:
clc;
% Simulation Parameters
T end = 100;
                   % Simulation time
                % Time step
dt = 0.01;
time = 0:dt:T_end; % Time vector
% System Parameters (Area 1 & Area 2)
[TG1, TG2] = deal(0.08, 0.06); % Governor time constants
[Tt1, Tt2] = deal(0.4, 0.44); % Turbine time constants
[TP1, TP2] = deal(20, 20);
                              % Power system time constants
[Kp1, Kp2] = deal(120, 115); % System gains
[Tii] = 0.2:
                       % Tie-line coefficient
[beta1, beta2] = deal(0.3483, 0.3827); % Frequency bias
% Uncertainty Factors
uncertainty_factor = 0.2;
                             % 20% uncertainty
TG1 = TG1 * (1 + uncertainty_factor);
TG2 = TG2 * (1 - uncertainty_factor);
% State-Space Matrices for Each Area
Ai = \dots
Bi = ...;
```

```
Ci = ...;
Di = \dots;
% Initial States
x1 = % State vector for Area 1
x2 = % State vector for Area 2
% Control Parameters
alpha = 0.9;
                 % Fractional order
c = 1.0;
               % Sliding surface coefficient
K = 5.0;
               % Switching gain
% Reinforcement Learning Initialization
RL agent = initialize RL(); % Custom RL agent initialization
% Disturbance Definition
disturbance 1 = @(t) (t > 20) * 0.05; % Load disturbance in Area 1
disturbance 2 = @(t) (t > 50) * -0.03; % Load disturbance in Area 2
% Simulation Loop
u1_log = zeros(size(time));
u2_log = zeros(size(time));
for k = 1:length(time)
  t = time(k);
  % Calculate Errors and ACE
  \begin{aligned} &ACE1 = C1 * x1 + Tij * (x1(3) - x2(3)); \\ &ACE2 = C2 * x2 + Tij * (x2(3) - x1(3)); \end{aligned}
  % Sliding Surfaces
  s1 = fractional_derivative(ACE1, alpha) + c * ACE1;
  s2 = fractional_derivative(ACE2, alpha) + c * ACE2;
  % Control Laws
  u1_eq = -inv(B1' * B1) * B1' * (A1 * x1 + disturbance1(t));
  u1_sw = -K * sign(s1);
  u1_RL = RL_agent.update_policy(s1, ACE1);
  u1 = u1_eq + u1_sw + u1_RL;
  u2 eq = -inv(B2' * B2) * B2' * (A2 * x2 + disturbance2(t));
  u2 \text{ sw} = -K * \text{sign}(s2);
  u2_RL = RL_agent.update_policy(s2, ACE2);
  u2 = u2_{eq} + u2_{sw} + u2_{RL};
  % Apply Control Inputs
  u1_{\log(k)} = u1;
  u2_log(k) = u2;
  % Update States
  dx1 = A1 * x1 + B1 * u1;
  dx2 = A2 * x2 + B2 * u2;
  x1 = x1 + dx1 * dt;
  x2 = x2 + dx2 * dt;
  % Update RL Agent
  reward1 = calculate_reward(ACE1, u1);
```

```
reward2 = calculate_reward(ACE2, u2);
RL_agent.learn(reward1, s1, ACE1);
RL_agent.learn(reward2, s2, ACE2);
end
% Plot Results
```

Appendix. B. The block diagram of the proposed method for controlling the two-area power system



Reference

- [1] F. Amiri & M.H. Moradi, Coordinated control of LFC and SMES in the power system using a new robust controller, Iranian Journal of Electrical and Electronic Engineering, 17(4) (2021) 1912-1912.
- [2] W. Ji, F. Hong, Y. Zhao, L. Liang, H. Du, J. Hao, ... & J. Liu, Applications of flywheel energy storage system on load frequency regulation combined with various power generations: A review, Renewable Energy, (2024) 119975.
- [3] F. Amiri & M.H. Moradi, Design of a new control method for dynamic control of the two-area microgrid, Soft Computing, 27(10) (2023) 6727-6747.
- [4] M.H. Moradi & F. Amiri, Improving the Stability of the Power System Based on Static Synchronous Series Compensation Equipped with Robust Model Predictive Control. Journal of Iranian Association of Electrical and Electronics Engineers.
- [5] H. Golpîra, H. Bevrani, A New Measurement-Based Approach for Power System Small Signal Stability and Voltage Regulation Enhancement, Journal of Iranian Association of Electrical and Electronics Engineers, 16(3) (2019) 61-72.
- [6] S. Wang, B. Li, G. Li, B. Li, H. Li, K. Jiao, & C. Wang, A Comprehensive Review on the Development of Data-Driven Methods for Wind Power Prediction and AGC Performance Evaluation in Wind-Thermal Bundled Power Systems, Energy and AI, (2024) 100336.
- [7] P. K. Vidyarthi, A. Kumar, A Modified Tilt Controller for AGC in Hybrid Power System Integrating Forecasting of Renewable Energy Sources, Optimal Control Applications and Methods, 45(1) (2024) 185-207.
- [8] F. Amiri, M. Eskandari, M. H. Moradi, Improved Load Frequency Control in Power Systems Hosting Wind Turbines by an Augmented Fractional Order PID Controller Optimized by the Powerful Owl Search Algorithm. Algorithms, 16(12) (2023) 539. https://doi.org/10.3390/a16120539.
- [9] Amiri, F., & M. H. Moradi, Improvement of Frequency Stability in the Power System Considering Wind Turbine and Time Delay. Journal of Renewable Energy and Environment, 10(1) (2023) 9-18. Doi: 10.30501/jree.2022.321859.1308.
- [10] M. Rajendran & S. Govindasamy, Performance Improvement of AGC Using Novel Controllers in a Multi-Area Solar Thermal System Under Deregulated Environment, Electric Power Components and Systems, 52(6) (2024) 847-862.
- [11] X. Liu, C. Wang, X. Kong, Y. Zhang, W. Wang, K. Y. & Lee, Tube-Based Distributed MPC for Load Frequency Control of Power System with High Wind Power Penetration, IEEE Transactions on Power Systems, 39(2) (2023) 3118-3129.
- [12] T. H. Mohamed, H. Bevrani, A. A. Hassan, & T. Hiyama, Decentralized Model Predictive-Based Load Frequency Control in an Interconnected Power System, Energy Conversion and Management, 52(2) (2011) 1208-1214.
- [13] J. Biswas, P. Bera, K. Chakrabarty, Determination of Control Area and Design of Fuzzy Rule-Tuned PID Controller for LFC of Multimachine Power System. Electric Power Systems Research, 221 (2023) 109411.
- [14] A. D. Shakibjoo, M. Moradzadeh, S. Z. Moussavi, A. Mohammadzadeh, L. Vandevelde, Load Frequency Control for Multi-Area Power Systems: A New Type-2 Fuzzy Approach Based on Levenberg–Marquardt Algorithm, ISA Transactions, 121 (2022) 40-52.
- [15] R. El-Sehiemy, A. Shaheen, A. Ginidi, S. F. Al-Gahtani, Proportional-Integral-Derivative Controller Based-Artificial Rabbits Algorithm for Load Frequency Control in Multi-Area Power Systems, Fractal and Fractional, 7(1) (2023) 97.
- [16] Z. Qu, W. Younis, X. Liu, A. K. Junejo, S. Z. Almutairi, P. Wang, Optimized PID Controller for Load Frequency Control in Multi-Source and Dual-Area Power Systems Using PSO and GA Algorithms, IEEE Access, (2024).
- [17] B. Dhanasekaran, J. Kaliannan, A. Baskaran, N. Dey, J. M. R. Tavares, Load Frequency Control Assessment of a PSO-PID Controller for a Standalone Multi-Source Power System, Technologies, 11(1) (2023) 22.
- [18] R. Kumar, V. K. Sharma, Interconnected Power Control on Unequal, Deregulated Multi-Area Power System Using Three-Degree-of-Freedom-Based FOPID-PR Controller. Electrical Engineering, 106(2) (2024) 2107-2129.
- [19] D. Sibtain, T. Rafiq, M. H. Bhatti, S. Shahzad, H. Kilic, Frequency Stabilization for Interconnected Renewable-Based Power System Using Cascaded Model Predictive Controller with Fractional Order PID Controller, IET Renewable Power Generation, 17(16) (2023) 3836-3855.
- [20] R. Kanimozhi, Load Frequency Control of Three-Area Power System Using Optimal Tuning of Fractional Order Proportional Integral Derivative Controller with Multi Objective Grey Wolf Optimization, Journal of Engineering Research, 11(2B) (2023)

10.22060/eej.2025.24314.5680

- [21] A. Jameel, M. M. Gulzar, Load Frequency Regulation of Interconnected Multi-Source Multi-Area Power System with Penetration of Electric Vehicles Aggregator Model, Electrical Engineering, 105(6) (2023) 3951-3968.
- [22] R. Kumar, A. Sikander, A Novel Load Frequency Control of Multi-Area Non-Reheated Thermal Power Plant Using Fuzzy PID Cascade Controller, Sādhanā, 48(1) (2023) 25.
- [23] Z. A. Ansari, G. L. Raja, Flow Direction Optimizer Tuned Robust FOPID-(1+ TD) Cascade Controller for Oscillation Mitigation in Multi-Area Renewable Integrated Hybrid Power System with Hybrid Electrical Energy Storage, Journal of Energy Storage, 83 (2024) 110616.
- [24] D. K. Biswas, S. Debbarma, P. P. Singh, LFC of Multi-Area Power System Using a Robust Full-Order Terminal Sliding Mode Controller Considering Communication Delay, Electrical Engineering, (2024) 1-15.
- [25] H. H. Alhelou, N. Nagpal, N. Kassarwani, P. Siano, Decentralized Optimized Integral Sliding Mode-Based Load Frequency Control for Interconnected Multi-Area Power Systems, IEEE Access, 11(2023) 32296-32307.
- [26] C. T. Nguyen, C. T. Hien, V. D. Phan, Observer-Based Single Phase Robustness Load Frequency Sliding Mode Controller for Multi-Area Interconnected Power Systems, Bulletin of Electrical Engineering and Informatics, 13(5) (2024) 3147-3154.
- [27] J. Guo, A Novel Proportional-Derivative Sliding Mode for Load Frequency Control, IEEE Access, (2024).
- [28] A. Gokyildirim, H. Calgan, M. Demirtas, Fractional-Order sliding mode control of a 4D memristive chaotic system, Journal of Vibration and Control, 30(7-8) (2024) 1604-1620.
- [29] H. Khan, S. Ahmed, J. Alzabut, A. T. Azar, J. F. Gómez-Aguilar, Nonlinear variable order system of multi-point boundary conditions with adaptive finite-time fractional-order sliding mode control, International Journal of Dynamics and Control, 1-17 (2024).
- [30] X. Yang, W. Chen, C. Yin, Q. Cheng, Fractional-Order Sliding-Mode Control and Radial Basis Function Neural Network Adaptive Damping Passivity-Based Control with Application to Modular Multilevel Converters, Energies, 17(3) (2024) 580.
- [31] D. Ernst, A. Louette, (2024). Introduction to reinforcement learning, (2024)111-126.
- [32] Z. Zhang, H. Li, T. Chen, N. N. Sze, W. Yang, Y. Zhang, G. Ren, Decision-making of autonomous vehicles in interactions with jaywalkers: A risk-aware deep reinforcement learning approach, Accident Analysis & Prevention, 210 (2025) 107843.
- [33] F. Amiri, S. Sadr, Improvement of Frequency Stability in Shipboard Microgrids Based on MPC-Reinforcement Learning, Journal of Electrical and Computer Engineering, 2025(1), 3139447.
- [34] F. Amiri, S. Sadr, Designing a New Control Method to Improve the LFC Performance of the Multi-Area Power System Considering the Effect of Offshore Wind Farms on Frequency Control, International Journal of Energy Research, 2025(1), 2737921.